Volume 5 | Number 7 | July 2018 | Pages 1521–1780

Environmental Science Nano

rsc.li/es-nano

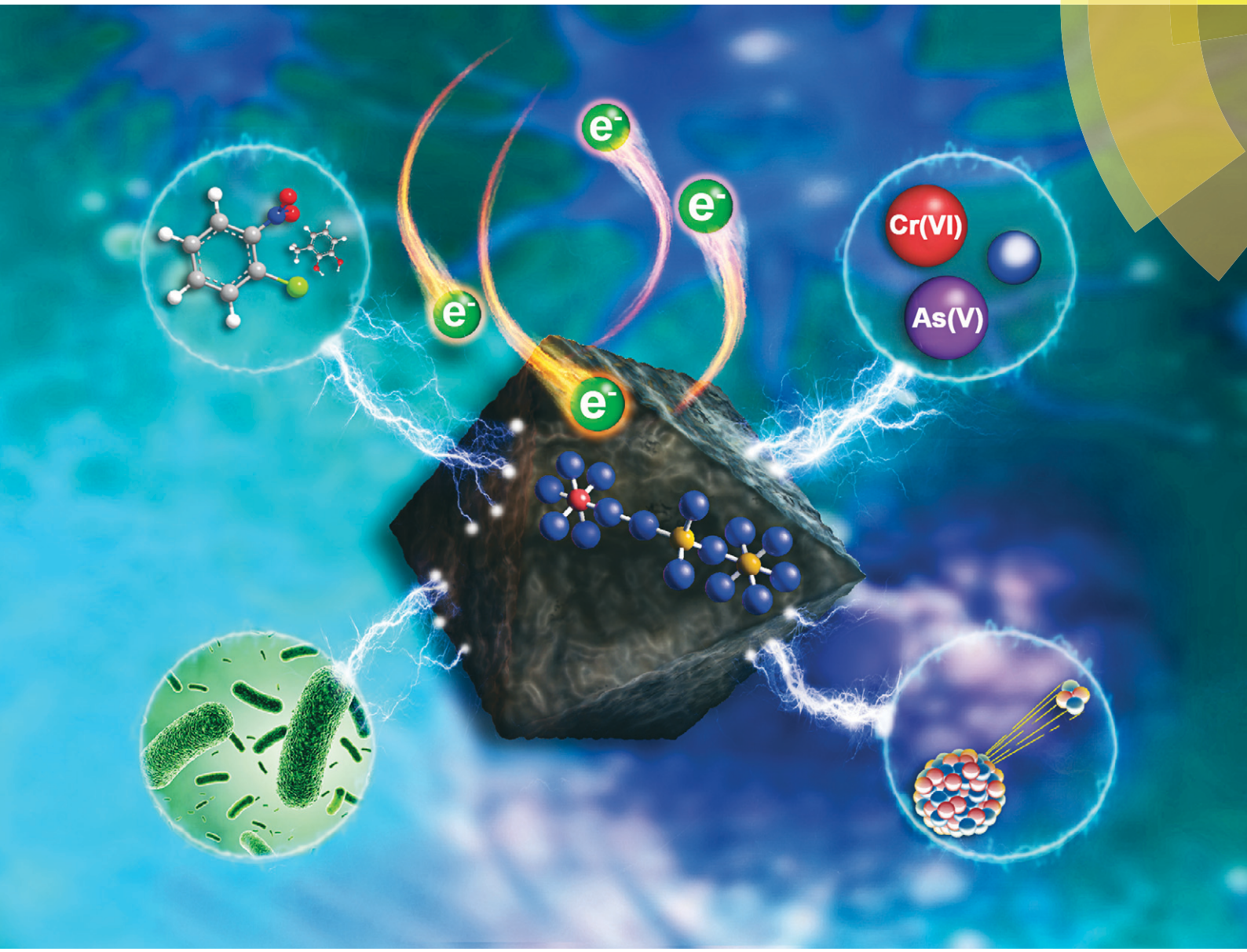

ISSN 2051-8153

ROYAL SOCIETY OF CHEMISTRY

PAPER
Juan Liu (PKU), Zhenli Zhu (CUG) *et al.*
Reversible Fe(II) uptake/release by magnetite nanoparticles

Environmental Science Nano

PAPER

View Article Online
View Journal | View Issue

Cite this: *Environ. Sci.: Nano*, 2018, 5, 1545

Reversible Fe(II) uptake/release by magnetite nanoparticles†

Huan Peng, [ab] Carolyn I. Pearce,[c] Weifeng Huang,[d] Zhenli Zhu, *[b] Alpha T. N'Diaye,[e] Kevin M. Rosso[c] and Juan Liu *[af]

Magnetite commonly coexists with aqueous Fe^{2+} ($Fe^{2+}_{(aq)}$) in anoxic subsurface environments. Complex interactions between magnetite and $Fe^{2+}_{(aq)}$ profoundly impact redox potential fluctuations in surrounding environment and biogeochemical cycles of important elements and contaminants. However, the ability of magnetite to act as a source/sink of electron equivalents through fluctuations in solution pH or the activity of $Fe^{2+}_{(aq)}$ remains poorly quantified. We systematically studied the interrelationships between equilibrium $Fe^{2+}_{(aq)}$ concentrations and structural *versus* surface-localized Fe(II)/Fe(III) ratios in magnetite using micro X-ray diffraction and synchrotron-based X-ray magnetic circular dichroism, respectively, under different controlled experimental conditions. Relative to pH 7, at pH 6 proton-promoted dissolution yields $Fe^{2+}_{(aq)}$ release from magnetite nanoparticles, coupled to a decrease in the structural Fe(II)/Fe(III) ratio by electron hopping along the octahedral sublattice from the particle interior to the surface. At pH 8, magnetite sorbs $Fe^{2+}_{(aq)}$, increasing both the structural and surface-localized Fe(II)/Fe(III) ratio. Amendments of $Fe^{2+}_{(aq)}$ inhibit acidic $Fe^{2+}_{(aq)}$ release and promote $Fe^{2+}_{(aq)}$ uptake at more basic conditions, whereas increasing magnetite loading facilitates $Fe^{2+}_{(aq)}$–magnetite interaction at the same respective pH extremes. The reversible flow of Fe(II) across the magnetite–solution interface under different conditions implies that the redox reactivity of magnetite nanoparticles is quickly responsive to changes in environmental conditions, such as an increase in pH due to groundwater passing through carbonate-rich rocks, *via* a dynamic redistribution of electron equivalents between particle interiors and the solid/water interface.

Received 21st March 2018,
Accepted 4th June 2018

DOI: 10.1039/c8en00328a

rsc.li/es-nano

Environmental significance

The coexistence of magnetite and $Fe^{2+}_{(aq)}$ is common in anoxic subsurface environments and can have a great influence on important biogeochemical redox processes. This study demonstrates that the flow direction of electron equivalents that in the form of Fe(II) across the magnetite–solution interface changes in a predictable fashion by altering solution pH, background $Fe^{2+}_{(aq)}$ concentration, and magnetite loading. The equilibrium distribution of Fe(II) in the magnetite–solution system, across a range of conditions relevant to natural aquatic environments, can significantly change the stoichiometry and reactivity of magnetite nanoparticles, and also may influence redox-cycling, contaminant transformation, and microbial extracellular respiration in surrounding environments.

1. Introduction

In anoxic aquifers, magnetite is one of the most common Fe(II)-containing minerals, playing an important role in a variety of biogeochemical processes, including immobilization of heavy metals and radioactive elements,[1,2] degradation or sorption of organic/inorganic contaminants,[3] and supplying electrons for microbial respiration.[4] Naturally occurring magnetite nanoparticles (NPs) can be generated *via* various biotic or abiotic processes.[5–7] In addition, increasing interest in the use of magnetite NPs for environmental treatments,[8] biomedical applications,[9] and many other industrial implications, may lead to the unintentional release of engineered magnetite NPs into the environment. Therefore, it is important to develop a more comprehensive understanding of the

[a] *The Key Laboratory of Water and Sediment Sciences, Ministry of Education, College of Environmental Sciences and Engineering, Peking University, Beijing 100871, China. E-mail: juan.liu@pku.edu.cn*
[b] *State Key Laboratory of Biogeology and Environmental Geology, School of Earth Sciences, China University of Geosciences, Wuhan, Hubei 430074, China. E-mail: zlzhu@cug.edu.cn*
[c] *Pacific Northwest National Laboratory, Richland, WA 99352, USA*
[d] *College of Engineering, Peking University, Beijing 100871, China*
[e] *Advanced Light Source, Lawrence Berkeley National Laboratory, Berkeley, CA 94720, USA*
[f] *Beijing Key Laboratory of Mineral Environmental Function, Peking University, Beijing 100871, China*

† Electronic supplementary information (ESI) available. See DOI: 10.1039/c8en00328a

transformation and reactivity of magnetite NPs in complex environmental systems.

The coexistence of magnetite and aqueous Fe^{2+} ($Fe^{2+}_{(aq)}$) is quite common in anoxic aquifers,[3,10] as a result of various biogeochemical processes, such as the weathering of Fe(II)-bearing minerals, abiotic reduction of Fe(III) (oxyhydr)oxides, and dissimilatory iron reduction.[11–13] Previous studies have suggested that the presence of $Fe^{2+}_{(aq)}$ may significantly influence the stoichiometry, reactivity, and recrystallization of magnetite NPs in aqueous environment.[3,14–16] The reaction of $Fe^{2+}_{(aq)}$ with magnetite NPs is of especially great interest in the field of environmental remediation, because the presence of magnetite NPs can distinctly enhance the reactivity of $Fe^{2+}_{(aq)}$ toward contaminant reduction.[3,14,17,18] Also, $Fe^{2+}_{(aq)}$ may react with magnetite surface and change mobility or redox state of heavy metals.[19,20] Despite its importance, molecular mechanisms of the interaction between $Fe^{2+}_{(aq)}$ and magnetite NPs have not been developed, in part due to the complexity of the magnetite/solution interface.[19]

To date, previous studies of the heterogeneous reactions between $Fe^{2+}_{(aq)}$ and iron oxides mainly focused on Fe(III)-(oxyhydr)oxides, such as goethite and hematite.[21–25] However, magnetite, as a mixed-valent iron oxide, can be expected to react with $Fe^{2+}_{(aq)}$ differently from Fe(III)-(oxyhydr)oxides, given its high electron mobility and facile topotactic interconversion with oxidized end-member maghemite.[1,2,26] Previous work focused on sorption isotherms and surface complexation models of $Fe^{2+}_{(aq)}$ on magnetite, as well as the reduction of contaminants by ferrous ions "sorbed on the magnetite surface".[27] However, recent experimental findings revealed that, in low temperature (<100 °C) aqueous systems, interfacial electron transfer occurs between sorbed Fe(II) and lattice Fe(III) in the underlying magnetite, followed by bulk electron conduction and the release of ferrous ions from other surface sites, *i.e.*, atom exchange.[27] In addition, Gorski *et al.* (2009) reported that the uptake of $Fe^{2+}_{(aq)}$ by partially oxidized magnetite at pH 7.2 increased the Fe(II)/Fe(III) ratio in the bulk magnetite structure and the corresponding reactivity of magnetite NPs.[3] However, the previous studies in this regard only examined a very limited range of conditions, such as a fixed magnetite loading at pH 7.2.[3,14] The extent of $Fe^{2+}_{(aq)}$–magnetite interaction and magnetite reactivity can be expected to vary substantially in response to fluctuating environmental conditions. For example, we have demonstrated in our previous work that the extent of Fe(II) release from (titano)magnetite decreases with increasing pH (pH = 6–8) but increases with the content of Ti substitution at a fixed pH.[1,4,26] Thus, to completely understand the role of magnetite NPs in natural environment, further studies are needed to systematically examine the correlation between the Fe(II)/Fe(III) ratio in magnetite structure and environmental variables.

Here we investigate the effects of solution pH, $Fe^{2+}_{(aq)}$ amendment, and magnetite loading on the Fe(II)/Fe(III) ratio, which together control the redox reactivity of magnetite NPs. In particular, we take advantage of sophisticated methods that we established in prior work to quantify the Fe(II)/Fe(III) ratio in particle interiors *versus* that in the outermost few Ångstroms of particle surfaces.[1,26] Micro X-ray diffraction (μXRD) was performed on anoxic NP aqueous suspensions before and after reactions with $Fe^{2+}_{(aq)}$ to infer the structural Fe(II)/Fe(III) ratio on the basis of the measured cell parameter. Synchrotron-based Fe L-edge X-ray absorption (XA) and magnetic circular dichroism (XMCD) spectroscopies were used to probe the Fe(II)/Fe(III) ratio at the surface and to distinguish tetrahedral and octahedral Fe(II) and Fe(III).[28] Corresponding equilibrium concentrations of $Fe^{2+}_{(aq)}$ in NP suspensions under various experimental conditions were measured using wet chemical analysis. Through systematic study of the relationship between $Fe^{2+}_{(aq)}$ concentration in solution and structural Fe(II)/Fe(III) in the bulk and at surfaces, reversible uptake and release of $Fe^{2+}_{(aq)}$ to and from sites in the magnetite structure was assessed as a function of solution pH, $Fe^{2+}_{(aq)}$ amendment, and magnetite loading. The findings provided insights into the equilibrium distribution of electron equivalents in the form of Fe(II) in the magnetite–solution system, across a range of conditions relevant to natural aquatic environments.

2. Materials and methods

2.1. Magnetite synthesis and characterization

Details about the chemical reagents and the anoxic glovebox used in this study are described in the ESI† (Section S1). Magnetite NPs were synthesized by a method modified from Pearce *et al.* 2012,[26] *via* co-precipitating a stoichiometric mixture of 0.1 M $FeCl_2{\cdot}4H_2O$ and 0.2 M $FeCl_3{\cdot}6H_2O$ (Fe^{2+} : Fe^{3+} mole ratio was 1 : 2) in the presence of ammonium (NH_4OH) solution in the glovebox. With continuous stirring, a N_2-sparged ammonium solution (28% w/v) was added dropwise to the chloride solution at ~60 °C, until precipitation was complete (pH = 9–11). After that, the suspension was continuously stirred for another 30 min. Finally, the NPs were magnetically separated from the suspension and then washed three times with degassed and deionized water (DDW) to remove excess iron salts. After the washing process, the NPs were re-suspended in DDW and stored inside the glovebox in dark. More details about the characterization of magnetite stoichiometry, NP concentration in the stock suspension, crystalline phase, particle size and morphology, as well as specific surface area (SSA) are described in Section S1.†

2.2. Heterogeneous reactions between $Fe^{2+}_{(aq)}$ and magnetite NPs

Concentration changes of dissolved ferrous ions ($[Fe^{2+}_{(aq)}]$) in the suspensions of 69–695 mg L^{-1} magnetite NPs (the equivalent Fe(II) concentration of 300–3000 μM) buffered at pH 6–8 with 0–1000 μM added $Fe^{2+}_{(aq)}$ over time were measured. The buffer solution at pH 6 was 30 mM MES solution, and that at pH 7 and 8 was 30 mM HEPES solution. Speciation distribution of 250–1000 μM $Fe^{2+}_{(aq)}$ in the buffer solution at pH 6–8 was calculated by Visual MINTEQ (Version 3.1,

Jon Petter Gustafsson, KHT, Div. of Land and Water Resources Engineering, Stockholm, Sweden). The results indicate that there is no significant difference in the speciation distribution of $Fe^{2+}_{(aq)}$ over the concentration range (0–1000 μM) studied (Table S1†). The reaction between $Fe^{2+}_{(aq)}$ and magnetite NPs was initiated by spiking a given volume of magnetite stock suspension to a buffer solution at the required pH and in presence of $FeSO_4$ with a desired concentration in 10 mL sealed bottles. The reactors were continuously shaken using a rotating overhead shaker at a speed of 10 rpm during reactions. Sample aliquots were taken over time and filtered using 0.22 μm syringe filters. [$Fe^{2+}_{(aq)}$] in the filtrates were determined by adding 0.2 mL of the filtrate to 1.8 mL ferrozine reagent (1 g L^{-1} ferrozine in 30 mM HEPES buffer, pH 7.0) and then measuring the absorbance at 562 nm by using a UV-visible spectrophotometer (Shimadzu UV-2501PC). All experiments were carried out at least in triplicates. The activity coefficient of $Fe^{2+}_{(aq)}$ in the pH 7.0 buffer solution for thermodynamic calculation was 0.6, which was calculated using extended Debye–Huckel model (Visual Minteq software, v3.0).

2.3. Micro X-ray diffraction (μXRD)

Crystalline phase and cell parameters of synthetic NPs before and after reaction with added $Fe^{2+}_{(aq)}$ were determined by μXRD using a Rigaku D/Max Rapid II instrument with a MicroMax 007HF generator fitted with a rotating Cr anode (λ = 2.2897 Å) and a 2D image plate detector. The XRD patterns were analyzed using JADE 9.0 from Materials Data Inc., and the PDF4+ database from ICSD. Samples for μXRD measurements were prepared by loading the concentrated NP suspensions into boron-rich 0.5 mm O.D. capillary tubes (Charles Supper Company) in the glovebox, and then sealing the capillaries with capillary wax (Charles Supper Company) to keep samples under anoxic conditions and in aqueous suspensions during measurements. The cell parameter of magnetite was obtained by fitting all strong diffraction peaks in XRD patterns using the pseudo-Voigt profile shape function. Based on the linear relationship between cell parameter and structural Fe(II)/Fe(III) ratio in magnetite,[26] the change of structural Fe(II)/Fe(III) ratio in magnetite NPs after reaction with $Fe^{2+}_{(aq)}$ was determined from the unit cell parameters measured using μXRD. The details of data processing and determination of cell parameters and structural Fe(II)/Fe(III) ratios were described previously.[26]

2.4. X-ray magnetic circular dichroism (XMCD)

To compare oxidation state and local structure of magnetically ordered iron cations at surface of magnetite NPs before and after the reactions with $Fe^{2+}_{(aq)}$, synchrotron XMCD spectra of magnetite NPs were collected at room temperature on beamline 6.3.1 at the Advanced Light Source (ALS), Berkeley, CA. Samples were prepared by drying aliquots of the NP suspensions onto carbon tape attached to the sample manipulator in an anoxic cabinet, which were maintained under anoxic conditions until immediately prior to XMCD measurements. X-ray absorption (XA) spectra at the Fe $L_{2,3}$ edges was collected in total-electron yield (TEY) mode with an effective probing depth of ~4.5 nm.[29] At each energy point, XA spectra were measured for two opposite magnetization directions by reversing the applied field of 0.4 T. The XMCD spectrum was obtained as the difference between these two XA spectra after normalization to the incident beam intensity.[30] The ratio of Fe(II) in octahedral coordination to Fe(III) in both tetrahedral and octahedral coordination was further calculated from XMCD spectra by means of a nonlinear least-squares analysis as described previously.[1,4,26]

3. Results and discussion

The XRD pattern (Fig. S1†) showed that the synthetic NPs were pure magnetite, and the representative TEM images (Fig. S2†) illustrated that they were ~10 nm in size and nearly spherical in shape. The BET result indicated that the specific surface area of the synthetic NPs was 55.7 m^2 g^{-1}. These characteristics are in good agreement with the properties of synthetic magnetite NPs reported in our previous studies.[1,2,4]

3.1. pH effects on $Fe^{2+}_{(aq)}$–magnetite interaction

Fig. 1A shows $Fe^{2+}_{(aq)}$ release from magnetite as a function of time in suspensions of 695 mg L^{-1} magnetite NPs ([Fe(II)] equivalent = 3 mM) at pH 6–8 without amended $Fe^{2+}_{(aq)}$. The measured [$Fe^{2+}_{(aq)}$] was nearly unchanged at pH 8 during the 24 h experiment, but at pH 6–7 [$Fe^{2+}_{(aq)}$] gradually increased

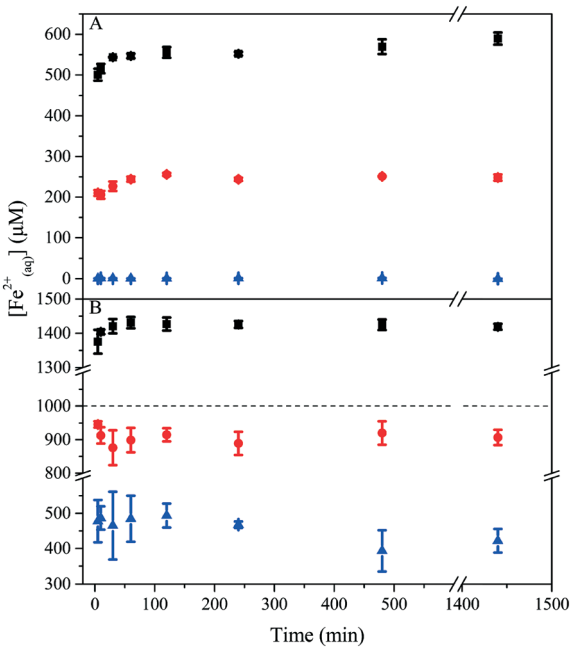

Fig. 1 Change of [$Fe^{2+}_{(aq)}$] as a function of time in the suspensions of magnetite NPs (3000 μM Fe(II) equivalent) at pH 6 (black), 7 (red), and 8 (blue), respectively, without amended $Fe^{2+}_{(aq)}$ (A) or in the presence of 1000 μM $Fe^{2+}_{(aq)}$ (B). The dashed line in (B) corresponds to [$Fe^{2+}_{(aq)}$] = 1000 μM.

with time and reached a plateau (~550 μM at pH 6 and ~250 μM at pH 7) after about 120 minutes. The results indicate that more $Fe^{2+}_{(aq)}$ ions were released from magnetite at a lower pH, which is consistent with the results of our previous study.[1] The stock suspension of synthetic magnetite NPs naturally equilibrated to pH ~ 8.5 after washing processes.[26] When an aliquot of the stock suspension was spiked into the buffer solution at pH 6 or 7, magnetite NPs were transferred from the stock suspension at pH ~ 8.5 to a buffer solution at a lower pH. The sudden pH decrease resulted in the release of $Fe^{2+}_{(aq)}$ from magnetite NPs into the aqueous phase due to the proton-promoted dissolution, as described by the equation:[1,31]

$$Fe^{3+}Fe^{3+}Fe^{2+}O_4^{2-} + 2H^+ \rightarrow \frac{3}{4}Fe^{3+}Fe_{5/3}^{3+}\square_{1/3}O_4^{2-} + H_2O + Fe^{2+} \quad (1)$$

The symbol □ represents a cationic vacancy due to diffusive migration of iron cations out of the octahedral sublattice. When the NP stock suspension was added to the buffer solution at pH 8, the pH change was insignificant, and accordingly a negligible amount of $Fe^{2+}_{(aq)}$ was released from magnetite.

When the 695 mg L^{-1} magnetite suspension was added to the pH 6–8 buffer solutions amended with 1000 μM $Fe^{2+}_{(aq)}$, the time-dependent concentrations of $Fe^{2+}_{(aq)}$ (Fig. 1B) were obviously different from those without $Fe^{2+}_{(aq)}$ amendment (Fig. 1A). In the pH 6 buffer solution amended with 1000 μM $Fe^{2+}_{(aq)}$, the values of $[Fe^{2+}_{(aq)}]$ increased with time and reached a stable value at ~1430 μM after ~60 min. Considering 1000 μM $Fe^{2+}_{(aq)}$ was initially added, 430 μM $Fe^{2+}_{(aq)}$ were released from 695 mg L^{-1} magnetite NPs under this condition, which was noticeably less than the value (550 μM) from magnetite without added $Fe^{2+}_{(aq)}$. As indicated by eqn (1) and Le Chatelier's principle, increasing the initial concentration/activity of $Fe^{2+}_{(aq)}$ can inhibit the extent of magnetite dissolution and thus decrease the amount of $Fe^{2+}_{(aq)}$ released from magnetite.

In the pH 7 buffer solution amended with 1000 μM $Fe^{2+}_{(aq)}$, $[Fe^{2+}_{(aq)}]$ slightly decreased with time and reached a stable value at ~900 μM after about 10 min (Fig. 1B), indicating the uptake of ~100 μM $Fe^{2+}_{(aq)}$ by 695 mg L^{-1} magnetite NPs. Thus, the addition of 1000 μM $Fe^{2+}_{(aq)}$ to the 695 mg L^{-1} magnetite suspension at pH 7 changed the dominant reaction from $Fe^{2+}_{(aq)}$ release to $Fe^{2+}_{(aq)}$ uptake. At pH = 8, $[Fe^{2+}_{(aq)}]$ fluctuated around 400 μM during the 24 h experiment, suggesting an instant uptake of ~600 μM $Fe^{2+}_{(aq)}$ by 695 mg L^{-1} magnetite NPs. The results indicate that the presence of 1000 μM $Fe^{2+}_{(aq)}$ inhibited Fe(II) release from magnetite at pH 6 and also promoted $Fe^{2+}_{(aq)}$ uptake at pH 7–8. The addition of 1000 μM $Fe^{2+}_{(aq)}$ at pH 7 not only changed the dominant interfacial reaction from $Fe^{2+}_{(aq)}$ release to $Fe^{2+}_{(aq)}$ uptake, but also shortened the time needed to reach equilibrium from ~120 min to ~60 min (Fig. 1).

Fig. 1 also shows that, under the experimental conditions in this study, the concentrations of $Fe^{2+}_{(aq)}$ reached a plateau in less than 24 hours. Previous studies also reported that the suspensions of iron oxide, such as magnetite, hematite, and goethite, reached equilibrium after 24 hour reaction with $Fe^{2+}_{(aq)}$.[3,32] Thus, equilibrium concentrations of $Fe^{2+}_{(aq)}$ in magnetite suspensions under different experimental conditions (pH = 6–8; initial $Fe^{2+}_{(aq)}$ concentrations = 0–1000 μM; NP loadings = 300–3000 μM [Fe(II)] equivalent) were measured after 24 hour reaction with $Fe^{2+}_{(aq)}$ (Fig. S3†). To compare reaction extents in different experiments, the difference between equilibrium concentration ($[Fe^{2+}_{(aq)}]_{equilibrium}$) and initial concentration ($[Fe^{2+}_{(aq)}]_{initial}$) of $Fe^{2+}_{(aq)}$, named as $\Delta[Fe^{2+}_{(aq)}]$ ($\Delta[Fe^{2+}_{(aq)}] = [Fe^{2+}_{(aq)}]_{equilibrium} - [Fe^{2+}_{(aq)}]_{initial}$), was plotted as a function of NP loadings in Fig. 2. Without added $Fe^{2+}_{(aq)}$, the values of $\Delta[Fe^{2+}_{(aq)}]$ in the systems with a fixed magnetite loading showed the order: pH 6 > pH 7 > pH 8 ≈ 0 (Fig. 2A). As mentioned above, the lower pH facilitated proton-promoted dissolution of magnetite, resulting in more $Fe^{2+}_{(aq)}$ released. Moreover, no matter how much $Fe^{2+}_{(aq)}$ was initially added or what magnetite loading was used, $\Delta[Fe^{2+}_{(aq)}]$ was always positive at pH 6 (Fig. 2B), confirming that proton-promoted dissolution was the dominant interfacial reaction at pH 6. On the contrary, at pH 8 and in the presence of added $Fe^{2+}_{(aq)}$, $\Delta[Fe^{2+}_{(aq)}]$ values were all negative, indicating that uptake of $Fe^{2+}_{(aq)}$ by magnetite was the dominant interfacial reaction in the pH 8 buffer solution amended with $Fe^{2+}_{(aq)}$ (Fig. 2D).

The tipping point in $\Delta[Fe^{2+}_{(aq)}]$ in our system was found to coincide at pH 7, where $\Delta[Fe^{2+}_{(aq)}]$ could be positive or negative depending on magnetite loading and initial $[Fe^{2+}_{(aq)}]$ (Fig. 2C). The results suggest that the dominant reaction between magnetite and $Fe^{2+}_{(aq)}$ at pH 7 could be switched between $Fe^{2+}_{(aq)}$ release and $Fe^{2+}_{(aq)}$ uptake simply by changing the ratio of initial $[Fe^{2+}_{(aq)}]$ (C_0) to magnetite loading (C_{Mt}). When the C_0/C_{Mt} ratio was less than ~0.5, $Fe^{2+}_{(aq)}$ release from magnetite NPs was the dominant reaction (Fig. 3). Otherwise, $Fe^{2+}_{(aq)}$ uptake was more favorable. The potential explanation for the reversible direction of electron equivalents ($Fe^{2+}_{(aq)}$) across the magnetite–solution interface at pH 7 will be discussed in section 3.4. The change of interfacial reactions in the range of pH 6–8 indicates that solution pH can significantly impact the distribution of electron equivalents between solution and magnetite, influencing the reductive reactivity of magnetite NPs.

3.2. Effects of NP loading and initial $[Fe^{2+}_{(aq)}]$ on $Fe^{2+}_{(aq)}$–magnetite interaction

When pH and initial $[Fe^{2+}_{(aq)}]$ were same, the absolute values of $\Delta[Fe^{2+}_{(aq)}]$ increased linearly with the increase of magnetite loading from 300 to 3000 μM at pH 6 and pH 8 (Fig. 2). As discussed above, the dominant reaction at pH 6 was proton-promoted dissolution of magnetite, which involves the initial binding of protons to surface oxygen atoms, weakening bridging Fe–O bonds, and the detachment of Fe(II) from the magnetite surface into solution.[33] Increasing magnetite loading can effectively elevate the concentration of Fe(II)

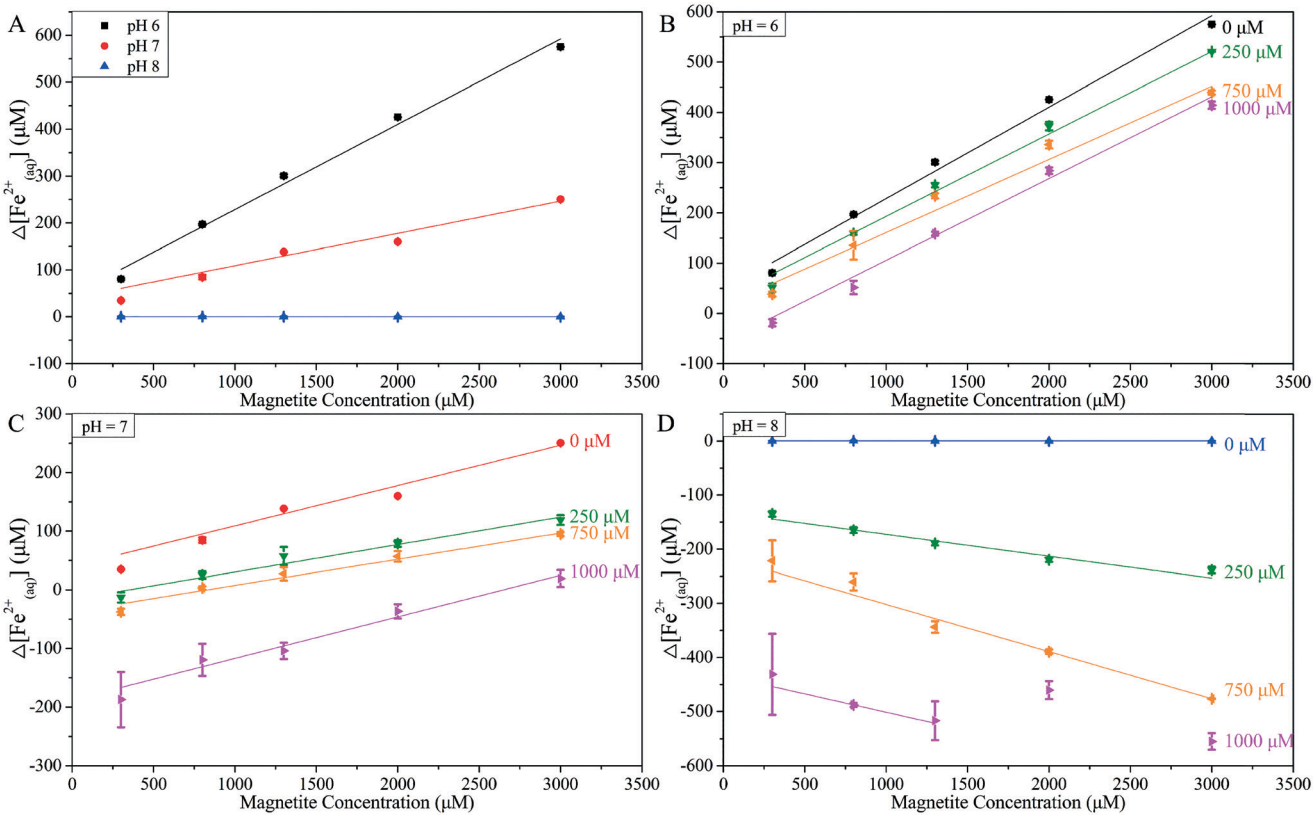

Fig. 2 The change of $\Delta[Fe^{2+}_{(aq)}]$ as a function of magnetite NPs loading without added $Fe^{2+}_{(aq)}$ (A), and in the presence of 0 μM (black), 250 μM (green), 750 μM (orange), or 1000 μM (magenta) $Fe^{2+}_{(aq)}$ at pH 6 (B), pH 7 (C), and pH 8 (D), respectively. The equation and R^2 of the fitted lines are shown in Table S2.†

introduced into the system in the form of NPs, which on the basis of eqn (1) shifts the equilibrium to the right, resulting in more $Fe^{2+}_{(aq)}$ released and the greater values of $\Delta[Fe^{2+}_{(aq)}]$ (Fig. 2B). As pH increased from 6 to 8, conversely the decreased acidity causes an equilibrium shift in the opposite direction whereupon the dominant reaction becomes $Fe^{2+}_{(aq)}$ uptake, which begins with the adsorption of $Fe^{2+}_{(aq)}$ onto magnetite surface, followed by interfacial electron transfer between sorbed Fe(II) and structural Fe(III).[34] Under this condition, the higher magnetite loading provided more active surface sites for $Fe^{2+}_{(aq)}$ adsorption and accordingly promoted $Fe^{2+}_{(aq)}$ uptake. As a result, the absolute values of $\Delta[Fe^{2+}_{(aq)}]$ were higher, as more magnetite NPs were added to the solution at pH 8 (Fig. 2D). Although increasing NP concentrations could change aggregation state of NPs, the continuous shaking in all experiments promoted the diffusion of $Fe^{2+}_{(aq)}$ onto magnetite surface and minimized the impact of NP aggregation on $Fe^{2+}_{(aq)}$–magnetite interaction.

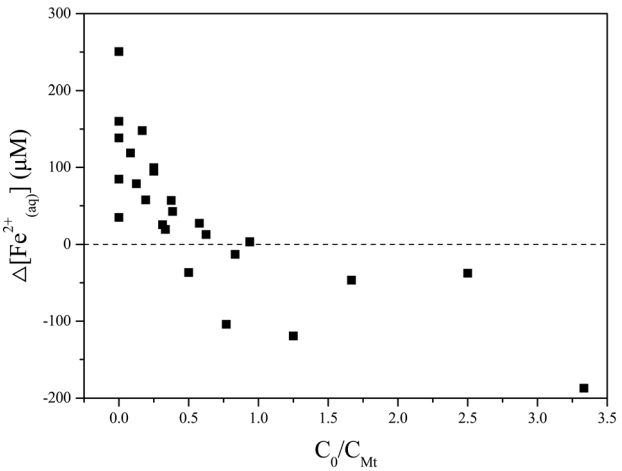

Fig. 3 $\Delta[Fe^{2+}_{(aq)}]$ *versus* the ratio of initial $[Fe^{2+}_{(aq)}]$ (C_0) to magnetite loading (C_{Mt}) at pH 7. Positive values of $\Delta[Fe^{2+}_{(aq)}]$ indicate Fe^{2+} release from magnetite NPs, whereas negative values represent Fe^{2+} uptake by magnetite NPs.

In all experiments, $\Delta[Fe^{2+}_{(aq)}]$ was linearly proportional to magnetite loading (Fig. 2). Table S2† shows the functions and *R*-squared values of all fitted regression lines in Fig. 2. The slopes of the fitted lines at pH 6 varied between 0.1455 and 0.1639 were independent of the concentration of added $Fe^{2+}_{(aq)}$. Compared to the slopes at pH 6, the absolute values of the corresponding slopes at pH 8 were obviously smaller (Table S2†). The difference might imply that the influence of NP loading was more significant on magnetite dissolution than on $Fe^{2+}_{(aq)}$ uptake by magnetite. The high *R*-squared values in all experiments confirmed the linear relationship between $\Delta[Fe^{2+}_{(aq)}]$ and magnetite loading, indicating that $Fe^{2+}_{(aq)}$–magnetite interaction under all of these conditions was a surface-mediated process, presumably limited by

available specific surface area. Aggregation state of magnetite was unlikely to significantly change as pH increased from 6 to 8, because extensive aggregation of magnetite NPs occurred at all these pH values due to a combination of Lifschitz–van der Waals and magnetic forces,[35] as well as the weak electrostatic repulsion between magnetite NPs at pH 6–8.[36] Thus, the observed pH effects on $Fe^{2+}_{(aq)}$–magnetite interaction could not be attributed to pH-dependent aggregation behavior of NPs.

To illustrate the effect of initial $[Fe^{2+}_{(aq)}]$ on magnetite–$Fe^{2+}_{(aq)}$ interaction, $\Delta[Fe^{2+}_{(aq)}]$ was replotted *versus* the initial concentration of added $Fe^{2+}_{(aq)}$ ($[Fe^{2+}_{(aq)}]_{add}$) (Fig. S4†). When NP loading and pH were fixed, there is a linear relationship between $\Delta[Fe^{2+}_{(aq)}]$ and $[Fe^{2+}_{(aq)}]_{add}$ under all experimental conditions in this study. At pH 6, the decrease in $\Delta[Fe^{2+}_{(aq)}]$ with increasing $[Fe^{2+}_{(aq)}]_{add}$ suggests the inhibition of magnetite dissolution by the additional $Fe^{2+}_{(aq)}$, as discussed above. In contrast, at pH 8, the higher initial $[Fe^{2+}_{(aq)}]$ led to the greater absolute values of $\Delta[Fe^{2+}_{(aq)}]$, indicating that the more added $Fe^{2+}_{(aq)}$ promoted $Fe^{2+}_{(aq)}$ uptake by magnetite NPs. As mentioned above, the adsorption of $Fe^{2+}_{(aq)}$ onto magnetite surface is a key step to initiate $Fe^{2+}_{(aq)}$ uptake by magnetite. Increasing the concentration of added $Fe^{2+}_{(aq)}$ could facilitate the adsorption of $Fe^{2+}_{(aq)}$ on magnetite surface. Moreover, in thermodynamic terms, increasing concentration of $Fe^{2+}_{(aq)}$ resulted in the lower reduction potential of aqueous solution. The difference in redox potentials between magnetite and solution tends to drive $Fe^{2+}_{(aq)}$ uptake by magnetite, in order to establish a new equilibrium at the solid/solution interface. Thus, the higher $[Fe^{2+}_{(aq)}]_{add}$ promoted $Fe^{2+}_{(aq)}$ uptake by magnetite NPs.

3.3. Structural Fe(II)/Fe(III) response

The extent to which this $Fe^{2+}_{(aq)}$ uptake and release by magnetite involves corresponding changes in structural Fe(II)/Fe(III) in the bulk was evaluated by performing μXRD measurements. As shown in Fig. S5,† the only crystalline phase observed in all μXRD patterns of post-reaction NPs was magnetite. Based on the known smooth relationship between cubic unit-cell length and magnetite stoichiometry, the structural Fe(II)/Fe(III) ratio in magnetite NPs was estimated directly from the measured cell parameter according to the method reported in previous studies.[26,37] The structural Fe(II)/Fe(III) ratios calculated from the μXRD patterns of 695 mg L^{-1} magnetite NPs ([Fe(II)] equivalent = 3000 μM) before and after reactions with 1000 μM $Fe^{2+}_{(aq)}$ at pH 6–8 were shown in Fig. 4 and Table 1. The results indicate that, irrespective of whether $Fe^{2+}_{(aq)}$ was initially added, the structural Fe(II)/Fe(III) ratio in the magnetite suspensions with the same initial $[Fe^{2+}_{(aq)}]$ and magnetite loading increased from pH 6 to pH 8. For example, at pH 8 without added $Fe^{2+}_{(aq)}$, the Fe(II)/Fe(III) ratio of magnetite NPs was 0.526 and obviously larger than the ratio (0.478) at pH 6 and that (0.498) at pH 7. This is consistent with the results, shown in Fig. 2, that low pH facilitates magnetite dissolution and

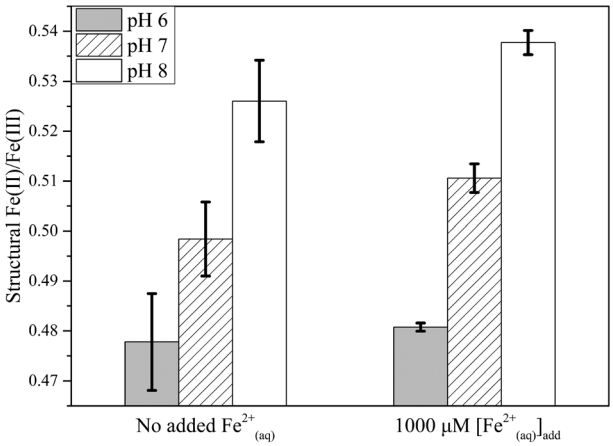

Fig. 4 Structural Fe(II)/Fe(III) ratios of magnetite NPs (695 mg L^{-1}) without added $Fe^{2+}_{(aq)}$ (left) and in the presence of 1000 μM $Fe^{2+}_{(aq)}$ (right), respectively, at pH 6, pH 7, and pH 8 from the measured lattice parameters by μXRD.

$Fe^{2+}_{(aq)}$ release from magnetite, whereas no detectable $Fe^{2+}_{(aq)}$ was released from magnetite at pH 8. Moreover, the addition of 1000 μM $Fe^{2+}_{(aq)}$ at pH 6–8 resulted in the higher structural Fe(II)/Fe(III) ratio, compared to the ratio of samples without added $Fe^{2+}_{(aq)}$. The trend agrees well with the results that $Fe^{2+}_{(aq)}$ amendment inhibited $Fe^{2+}_{(aq)}$ release from magnetite at low pH and promoted $Fe^{2+}_{(aq)}$ uptake by magnetite at high pH (Fig. 2). The Fe^{2+} content in the solid is thus highly mobile and responsive to changes in chemical potential at the magnetite–solution interface.

It is worth mentioning that under some conditions a hyperstoichiometric "cation-excess" magnetite was formed. For example, at pH 8, the addition of 1000 μM $Fe^{2+}_{(aq)}$ increased the structural Fe(II)/Fe(III) ratio well beyond 0.5 (Table 1). The exact physical nature of this condition remains unclear. In previous studies, uptake of $Fe^{2+}_{(aq)}$ by magnetite NPs at elevated pH has been simply attributed to the increasing adsorption capacity for $Fe^{2+}_{(aq)}$. The point of zero charge of magnetite is 6.4–6.85,[14,36,38] so increasing pH from 6 to 8 can lead to more negative surface that might adsorb more $Fe^{2+}_{(aq)}$ non-specifically *via* electrostatic attraction.[14] However, Gorski *et al.* (2009) reported that no stable sorbed Fe(II) species was observed on magnetite NPs after exposure to $Fe^{2+}_{(aq)}$ at pH 7.2. They further showed that $Fe^{2+}_{(aq)}$ can incorporate into the structure of partially oxidized or nonstoichiometric magnetite, and the extent of $Fe^{2+}_{(aq)}$ uptake is limited by the formation of stoichiometric magnetite (Fe(II)/Fe(III) = 0.5). This conclusion was based on the experiments with a constant magnetite loading (1 g L^{-1}) at pH 7.2. The results of the present study indicate that increasing pH or initial $[Fe^{2+}_{(aq)}]$ can promote $Fe^{2+}_{(aq)}$ uptake and result in a Fe(II)/Fe(III) beyond 0.5. This hyperstoichiometry may possibly indicate incorporation of ferrous ions into minor cation vacancies in the octahedral sublattice, or the reduction of octahedral Fe(III) by injected electrons from sorbed Fe(II).[27,39]

In addition to the structural Fe(II)/Fe(III) ratio in the bulk as shown by μXRD, the Fe(II)/Fe(III) ratio in the near-surface

Table 1 The change of $Fe^{2+}_{(aq)}$ concentration ($\Delta[Fe^{2+}_{(aq)}]$), the structural Fe(II)/Fe(III) ratio in magnetite NPs calculated from μXRD results, and the surface-localized XMCD Fe(II)/Fe(III) ratio in magnetite NPs before and after reaction with $Fe^{2+}_{(aq)}$ at pH 6–8. The magnetite loading in all experiments was 695 mg L^{-1}

		Ferrozine	Lattice parameters	Micro-XRD	XMCD
pH	$[Fe^{2+}_{(aq)}]_{add}$ (μM)	$\Delta[Fe^{2+}_{(aq)}]^a$ (μM)	Å	Fe(II)/Fe(III)	Fe(II)/Fe(III)
Original	0	—	8.4050	0.544	0.538
6	0	575	8.3981	0.478	—
	1000	414	8.3984	0.481	—
7	0	250	8.4003	0.498	0.604
	500	150	—	—	0.754
	1000	19	8.4015	0.511	0.714
8	0	0	8.4031	0.526	0.593
	500	−425	—	—	0.634
	1000	−555	8.4043	0.538	0.610

[a] Negative values in $\Delta[Fe^{2+}_{(aq)}]$ represent Fe^{2+} uptake to magnetite, and positive values represent Fe^{2+} release from magnetite.

region was independently probed using Fe L-edge XAS and XMCD (Fig. 5 and Table 1). In contrast to μXRD, the information depth of XAS/XMCD is no more than 4.5 nm, with sensitivity that exponentially increases to the outermost surface atoms. Furthermore, whereas XAS detects all iron within this near-surface region, XMCD is sensitive only to the magnetically ordered Fe(II) and Fe(III), thus selecting primarily for iron sites in lattice positions at the surface.[28] When 695 mg L^{-1} magnetite NPs were exposed to the pH 7 buffer solution without $Fe^{2+}_{(aq)}$ amendment, the surface Fe(II)/Fe(III) ratio increased from 0.538 to 0.604, while the structural Fe(II)/Fe(III) ratio decreased from 0.544 to 0.498 (Table 1). The opposite trends likely indicate solid-state migration of electrons from the interior to the near-surface region, as has been previously observed during the acidic dissolution of magnetite NPs and microparticles.[4,26,28]

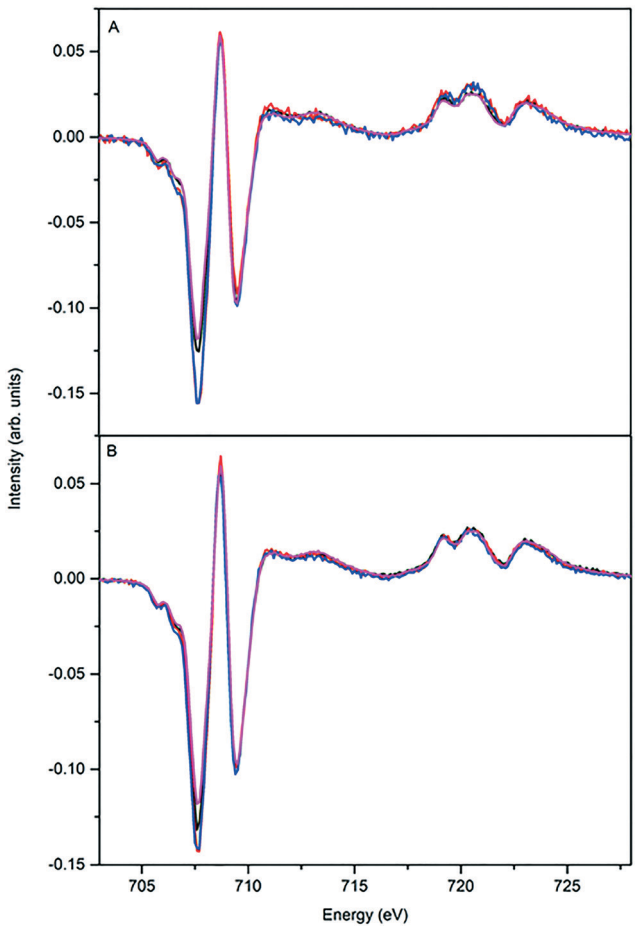

Fig. 5 Comparison of XMCD spectra of magnetite NPs in stock suspension (magenta), in the buffer solution (black), and in the buffer solution with 500 μM (red) or 1000 μM (blue) added $Fe^{2+}_{(aq)}$ at pH 7 (A) and 8 (B).

When 500 μM $Fe^{2+}_{(aq)}$ were initially added at pH 7, $\Delta[Fe^{2+}_{(aq)}]$ was 150 μM, indicating that magnetite dissolution was the dominant reaction. However, the surface-localized Fe(II)/Fe(III) ratio became 0.754 that was evidently higher than the ratios of magnetite in the stock suspension (0.538) or in the pH 7 buffer solution without added $Fe^{2+}_{(aq)}$ (0.604) (Table 1). The presence of 500 μM $Fe^{2+}_{(aq)}$ worked against proton-promoted dissolution of magnetite, and the $Fe^{2+}_{(aq)}$ amendment induces further enrichment of Fe(II) in the near-surface region. When the concentration of $Fe^{2+}_{(aq)}$ was increased to 1000 μM, $\Delta[Fe^{2+}_{(aq)}]$ decreased from 150 to 19 μM, indicating a stronger inhibition of dissolution. However, the surface-localized Fe(II)/Fe(III) ratio was no longer observed to increase by XMCD, suggesting that the limit for Fe(II) enrichment into surface structure had been reached. Once saturated, the relatively high surface-localized Fe(II)/Fe(III) ratio might also suggest that further participation of Fe(II) from particle interiors in interfacial electron transfer may also saturate.

At pH 8, the surface-localized Fe(II)/Fe(III) ratio of magnetite NPs was also in the order: stock suspension < buffer solution without added $Fe^{2+}_{(aq)}$ < buffer solution with 1000 μM $Fe^{2+}_{(aq)}$. When NPs were exposed to the pH 8 buffer solution without additional $Fe^{2+}_{(aq)}$, no measurable $Fe^{2+}_{(aq)}$ was released from NPs, but the structural Fe(II)/Fe(III) ratio decreased from 0.544 to 0.526 as shown in Table 1. Simultaneously, the surface-localized Fe(II)/Fe(III) ratio of magnetite NPs increased from 0.538 to 0.593. Although no change in the concentration of $Fe^{2+}_{(aq)}$ was observed under this condition, Fe(II) enriched at the near-surface region of magnetite

NPs as a result of transferring NPs from the stock suspension to the pH 8 buffer solution. When 1000 μM $Fe^{2+}_{(aq)}$ was added at pH 8, the structural Fe(II)/Fe(III) ratio increased from 0.526 to 0.538, and the surface-localized Fe(II)/Fe(III) ratio increased from 0.593 to 0.610 (Table 1). The results might suggest that $Fe^{2+}_{(aq)}$ incorporation or electron injection occurred both at the near-surface region and in particle interiors under this condition, resulting in the distribution of excess Fe(II) throughout the hyperstoichiometric magnetite NPs. In the XAS in general, the $L_{2,3}$-edge for Fe exhibits a shift to higher energy with an increase in oxidation state. Fig. 6 shows that the lower energy Fe $L_{2,3}$-edge peak intensity at 707.8 eV increased as $Fe^{2+}_{(aq)}$ was added, corresponding to an increase the total ferrous Fe concentration at the surface of the NPs. The increase in intensity of the first peak (~707.8 eV) in XMCD spectrum in Fig. 5 corresponds to Fe(II) in octahedral coordination and demonstrates that the high Fe(II)/Fe(III) is truly a gradient within the magnetite structure. If the Fe(II) was surface sorbed in a non-specific or poorly ordered manner, it would be detectable by an increase in the low energy peak intensity in the XA without a corresponding increase in the first peak in the XMCD. Moreover, no secondary crystalline phases were observed by μXRD in all samples after reaction with $Fe^{2+}_{(aq)}$. Thus, the higher Fe(II)/Fe(III) ratio shown in XMCD spectra can be attributed to changes in the composition of the structural iron at the near-surface after reaction, and not to secondary phases or adsorbed iron complexes.

3.4. Redistribution of Fe(II) as a result of $Fe^{2+}_{(aq)}$–magnetite interaction

Attempts were made to quantify the mass and electron balanced redistribution of Fe(II) between the aqueous phase, particle interiors, and particle surfaces, as a function of system variables, based on the results of this study. For example, μXRD results showed that the Fe(II)/Fe(III) ratio of magnetite in the stock suspension of synthetic NPs was 0.544 (Table 1). When the magnetite loading was 695 mg L^{-1} ([Fe(II)] equivalent = 3 mM), the concentrations of structural Fe(II) and Fe(III) in as-synthesized magnetite NPs were 3000 μM and 5516 μM, respectively (Table 2). After exposed to the pH 7 buffer solution without added $Fe^{2+}_{(aq)}$, the Fe(II)/Fe(III) ratio of magnetite decreased to 0.498, and $\Delta[Fe^{2+}_{(aq)}]$ was 250 μM. As mentioned above, no stable sorbed Fe(II) species were observed on NP surfaces after reaction with $Fe^{2+}_{(aq)}$ at pH 7,[3] and no secondary crystalline phase was observed in the μXRD patterns of post-reaction samples. Thus, $\Delta[Fe^{2+}_{(aq)}]$ in solution presumably equaled the decrease of total Fe concentration ($[Fe_{tot}]$) in NPs at equilibrium. As 250 μM $Fe^{2+}_{(aq)}$ ($\Delta[Fe^{2+}_{(aq)}]$ = 250 μM) was released from 695 mg L^{-1} magnetite NPs after the NPs were transferred from the stock suspension to the pH 7 buffer solution, the total Fe ($[Fe_{tot}]$) in the magnetite NPs accordingly decreased from 8516 to 8266 μM (Table 2). The μXRD results show that the structural Fe(II)/Fe(III) ratio of magnetite NPs was 0.498 in the pH 7 buffer solution without amended $Fe^{2+}_{(aq)}$ (Table 1), so the concentration of Fe(II) in magnetite structure was 2748 μM that was 252 μM less than the structural Fe(II) concentration (3000 μM) in 695 mg L^{-1} as-synthesized magnetite NPs (Table 2). The results indicate that the increase of $Fe^{2+}_{(aq)}$ concentration ($\Delta[Fe^{2+}_{(aq)}]$) from chemical analysis was very close to the decrease of structural Fe(II) in magnetite NPs ($\Delta[Fe(II)_{str}]$) measured by μXRD. The good consistency confirmed that, at pH 7 and without added $Fe^{2+}_{(aq)}$, the increase of $[Fe^{2+}_{(aq)}]$ in solution was mainly attributed to Fe(II) release from magnetite structure. Moreover, the concentration of structural Fe(III) in magnetite was nearly unchanged after reaction under this condition.

However, when 1000 μM $Fe^{2+}_{(aq)}$ was initially added in pH 7 buffer solution, $\Delta[Fe^{2+}_{(aq)}]$ was only 19 μM, indicating the corresponding total Fe in NPs was 8497 μM. The μXRD results showed the Fe(II)/Fe(III) ratio of NPs in this case was 0.511, so the concentrations of structural Fe(II) and Fe(III) were 2874 μM and 5623 μM, respectively. Compared to as-synthesized NPs, the equivalent concentration of structural Fe(II) decreased 126 μM, but that of structural Fe(III) increased 107 μM (Table 2). This

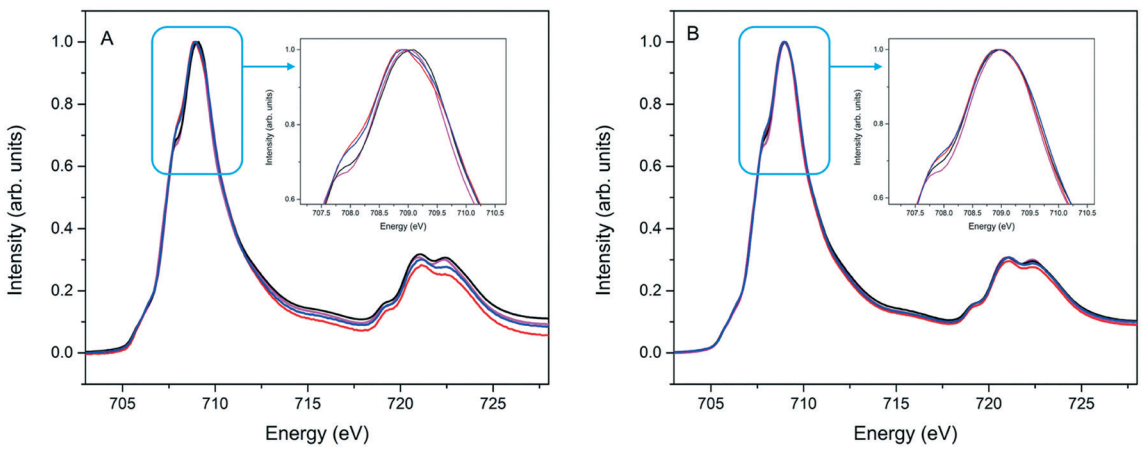

Fig. 6 Comparison of XAS spectra of magnetite NPs in stock suspension (magenta), in the buffer solution (black), and in the buffer solution with 500 μM (red) or 1000 μM (blue) added $Fe^{2+}_{(aq)}$ at pH 7 (A) and 8 (B).

Table 2 Changes of $Fe^{2+}_{(aq)}$ concentration based on chemical analysis and structurally ordered Fe(II) in NPs measured by μXRD

pH	$[Fe^{2+}_{(aq)}]_{added}$ [a] (μM)	$\Delta[Fe^{2+}_{(aq)}]$ [b] (μM)	$[Fe(II)_{str}]$ [c] (μM)	$[Fe(III)_{str}]$ [d] (μM)	$[Fe_{tot}]$ [e] (μM)	$\Delta[Fe(II)_{str}]$ [f] (μM)
Original	0	0	3000	5516	8516	—
7	0	250	2748	5518	8266	−252
7	1000	19	2874	5623	8497	−126

[a] The concentration of $Fe^{2+}_{(aq)}$ that was initially added. [b] The difference between equilibrium and initial concentrations of $Fe^{2+}_{(aq)}$. [c] The concentration of structural Fe(II) equivalent in magnetite NPs equilibrated with the pH 7 buffer solution, which was calculated from the μXRD results in Table 1. [d] The concentration of structural Fe(III) equivalent in magnetite NPs equilibrated with the pH 7 buffer solution. [e] $[Fe_{tot}] = [Fe(II)_{str}] + [Fe(III)_{str}]$. [f] The change of structural Fe(II) concentration after equilibrated at pH 7 with or without added $Fe(II)_{(aq)}$.

suggests that charge redistribution between Fe(II) and Fe(III) in the magnetite structure might happen concurrently with proton-promoted dissolution in the pH 7 buffer solution amended with 1000 μM $Fe^{2+}_{(aq)}$. The calculation above was based on the assumption that there were negligible amounts of amorphous iron-containing solid phase formed in the system at equilibrium. Although the μXRD and XMCD results in this study could not rule out the formation of iron-containing amorphous phases, the representative TEM image of magnetite NPs after reaction with $Fe^{2+}_{(aq)}$ at pH 7 (Fig. S6†) did not show the presence of amorphous phases. Moreover, previous experimental studies have suggested that no stable, adsorbed iron complexes or phases on iron oxide surfaces after reaction with $Fe^{2+}_{(aq)}$ under anaerobic conditions at pH 7.[3,21,22,25,33,39–41] Nevertheless, more detailed studies on iron speciation as a result of magnetite–$Fe^{2+}_{(aq)}$ interaction under different experimental conditions are needed, in order to precisely describe the distribution of Fe(II) and electrons at the interface between magnetite and $Fe^{2+}_{(aq)}$.

The findings in this study showed that $Fe^{2+}_{(aq)}$ uptake or release can occur in the $Fe^{2+}_{(aq)}$–magnetite system depending on pH, initial $Fe^{2+}_{(aq)}$ concentration, and NP loading. The flow direction of electron equivalents in the form of Fe(II) across the $Fe^{2+}_{(aq)}$–magnetite interface can be determined by the difference in redox potentials between magnetite and solution. For example, when 800 μM magnetite NPs equilibrated with the pH 7 buffer solution amended with 750 μM $Fe^{2+}_{(aq)}$, $\Delta[Fe^{2+}_{(aq)}]$ was 3.1 μM that was close to zero (Fig. 2C). The change of structural Fe(II)/Fe(III) in magnetite under this condition was negligible. Because the redox potentials of magnetite and solution must equal to each other at equilibrium, the redox potential of 800 μM magnetite at pH 7 can be estimated from the equilibrium concentration of $Fe^{2+}_{(aq)}$.[32] The half-reaction between $Fe^{2+}_{(aq)}$ and magnetite can be written as:[42]

$$0.5Fe_3O_4 + 4H^+ + e^- \rightarrow 1.5Fe^{2+} + 2H_2O \quad (2)$$

By assuming that the activities of water and magnetite are 1, at room temperature (298 K), the corresponding Nernst equation can be written as follows:

$$E_H = E_H{}^0 - 88.5\log\{Fe^{2+}_{(aq)}\} - 236\ pH \quad (3)$$

where $E_H{}^0$ equals 1090 mV *vs.* SHE;[42] $\{Fe_{(aq)}{}^{2+}\}$ is the activity of $Fe^{2+}_{(aq)}$ at equilibrium; E_H is the reduction potential of magnetite suspension with $Fe^{2+}_{(aq)}$ at a given pH. Thus, the redox potential of 800 μM magnetite NPs at pH 7 was close to −266 mV. When the initial $[Fe^{2+}_{(aq)}]$ increased from 750 to 1000 μM, the calculated E_H value of solution according to eqn (3) was lower than −266 mV. To reach equilibrium under this condition, $Fe^{2+}_{(aq)}$ uptake happened, in order to decrease $Fe^{2+}_{(aq)}$ concentration and correspondingly increase E_H of solution. Because redox potential of magnetite is inversely proportional to structural Fe(II)/Fe(III) ratio in magnetite, $Fe^{2+}_{(aq)}$ uptake by magnetite could increase structural Fe(II)/Fe(III) ratio and also decrease redox potential of magnetite NPs. Therefore, the flow of electron equivalents from solution to magnetite could effectively reduce the difference in the redox potentials between solution and magnetite, until a new equilibrium was reached. On the other hand, increasing magnetite loading can lead to a lower reduction potential of magnetite suspension.[15] When magnetite loading was higher than 800 μM at pH 7 and with 750 μM added $Fe^{2+}_{(aq)}$, the redox potential of magnetite was lower than −266 mV. In this case, $Fe^{2+}_{(aq)}$ release from magnetite to solution could minimize the difference in redox potentials between magnetite NPs and aqueous solution. The findings in this study suggest that the subtle alteration of solution conditions or magnetite loading may disrupt the equilibrium at the magnetite–solution interface and drive the redistribution of Fe(II), in the form of $Fe^{2+}_{(aq)}$ release or uptake, until a new equilibrium is reached. The dynamic redistribution of electron equivalents also produces a challenge to experimentally quantify the reduction potential of magnetite NPs, which can be quite distinct under different solution conditions or particle loadings.

4. Conclusions

Magnetite, as a common iron oxide in the environment with high reactivity and good biocompatibility, has been widely studied in a variety of environmental contexts and applications. The coexistence of magnetite and $Fe^{2+}_{(aq)}$ is pervasive in anoxic aquifers, resulting from various biogeochemical processes. Moreover, recharging magnetite with $Fe^{2+}_{(aq)}$ has been considered as an efficient way to trigger or enhance its reactivity in environmental remediation. This study presents the first systematic work examining the effects of pH, initial $Fe^{2+}_{(aq)}$ concentration, and magnetite loading on the distribution of electron equivalents in terms of Fe(II) between $Fe^{2+}_{(aq)}$ and magnetite NPs at circumneutral pH. Increasing pH from

6 to 8 changed the primary reaction between magnetite NPs and $Fe^{2+}_{(aq)}$ from proton-promoted dissolution to $Fe^{2+}_{(aq)}$ uptake, which is accompanied by an increase of the bulk structural Fe(II)/Fe(III) ratio in magnetite NPs. $Fe^{2+}_{(aq)}$ amendments inhibit magnetite dissolution at pH 6 and promote $Fe^{2+}_{(aq)}$ uptake at elevated pH, whereas the addition of more magnetite NPs can lead to $Fe^{2+}_{(aq)}$ release and uptake through shifts in the balance between two effects - increasing the available Fe^{2+} in the system while also increasing the solid specific surface area.

The findings in this study show that the reversible $Fe^{2+}_{(aq)}$ uptake/release by magnetite NPs can be controlled by altering environmental variables, such as solution pH, $Fe^{2+}_{(aq)}$ concentration, or magnetite loading. This study underscores the ability of magnetite to act as a rechargeable "battery" that couples to the redox-cycling of elements and transformation of contaminants in redox-oscillating environments. This role for magnetite appears to promote microbial respiration[43] and stimulate direct interspecies electron transfer (DIET) in syntrophic microbial communities.[36] Thus, the changes of surface-localized and structural Fe(II)/Fe(III) ratios as a result of $Fe^{2+}_{(aq)}$–magnetite interaction under varied environmental conditions may also impact the related microbial metabolisms.

The stoichiometry and reduction reactivity of magnetite NPs can be substantially altered due to slight changes of environmental conditions. The results of this study also provide insights into the variable reactivity of magnetite NPs in natural environments and provide a foundation for tailoring magnetite reactivity in NPs or as coatings on zero-valent iron (ZVI) for environmental remediation.

Conflicts of interest

There are no conflicts of interest to declare.

Acknowledgements

This work was financially supported by National Basic Research Program of China (973 Program, 2014CB846001) and National Natural Science Foundation of China (41472306, 41230103, and 21375120). KMR acknowledges support from the U.S. Department of Energy (DOE), Office of Science, Office of Basic Energy Sciences, from the Chemical Sciences, Geosciences, and Biosciences Division through its Geosciences program at Pacific Northwest National Laboratory (PNNL). A portion of this research was performed using EMSL, a national scientific user facility sponsored by the DOE Office of Biological and Environmental Research and located at PNNL. The work performed at the ALS is supported by the Director, Office of Basic Energy Sciences of the U.S. DOE under Contract No. DE-AC02-05CH11231. We thank Dr. Xin Zhang at PNNL for taking TEM images of magnetite NPs.

Notes and references

1 J. Liu, C. I. Pearce, O. Qafoku, E. Arenholz, S. M. Heald and K. M. Rosso, Tc(VII) reduction kinetics by titanomagnetite ($Fe_{3-x}Ti_xO_4$) nanoparticles, *Geochim. Cosmochim. Acta*, 2012, **92**, 67–81.

2 C. I. Pearce, J. Liu, D. R. Baer, O. Qafoku, S. M. Heald, E. Arenholz, A. E. Grosz, J. P. McKinley, C. T. Resch, M. E. Bowden, M. H. Engelhard and K. M. Rosso, Characterization of natural titanomagnetites ($Fe_{3-x}Ti_xO_4$) for studying heterogeneous electron transfer to Tc(VII) in the Hanford subsurface, *Geochim. Cosmochim. Acta*, 2014, **128**, 114–127.

3 C. A. Gorski and M. M. Scherer, Influence of magnetite stoichiometry on Fe^{II} uptake and nitrobenzene reduction, *Environ. Sci. Technol.*, 2009, **43**, 3675–3680.

4 J. Liu, C. I. Pearce, C. Liu, Z. Wang, L. Shi, E. Arenholz and K. M. Rosso, $Fe_{3-x}Ti_xO_4$ nanoparticles as tunable probes of microbial metal oxidation, *J. Am. Chem. Soc.*, 2013, **135**, 8896–8907.

5 R. M. Cornell and U. Schwertmann, *The Iron Oxides: Structure, Properties, Reactions, Occurrences and Uses*, Wiley-VCH, Weinheim, 2003.

6 D. C. Smith and B. McEnaney, The influence of dissolved oxygen concentration on the corrosion of grey cast iron in water at 50°C, *Corros. Sci.*, 1979, **19**, 379–394.

7 T. Ahn, J. H. Kim, H.-M. Yang, J. W. Lee and J.-D. Kim, Formation Pathways of Magnetite Nanoparticles by Coprecipitation Method, *J. Phys. Chem. C*, 2012, **116**, 6069–6076.

8 P. Xu, G. M. Zeng, D. L. Huang, C. L. Feng, S. Hu, M. H. Zhao, C. Lai, Z. Wei, C. Huang, G. X. Xie and Z. F. Liu, Use of iron oxide nanomaterials in wastewater treatment: A review, *Sci. Total Environ.*, 2012, **424**, 1–10.

9 Q. A. Pankhurst, J. Connolly, S. K. Jones and J. Dobson, Applications of magnetic nanoparticles in biomedicine, *J. Phys. D: Appl. Phys.*, 2003, **36**, R167–R181.

10 V. Tishchenko, C. Meile, M. M. Scherer, T. S. Pasakarnis and A. Thompson, Fe^{2+} catalyzed iron atom exchange and recrystallization in a tropical soil, *Geochim. Cosmochim. Acta*, 2015, **148**, 191–202.

11 B. Zinder, G. Furrer and W. Stumm, The coordination chemistry of weathering: II. Dissolution of Fe(III) oxides, *Geochim. Cosmochim. Acta*, 1986, **50**, 1861–1869.

12 C. Colombo, G. Palumbo, J.-Z. He, R. Pinton and S. Cesco, Review on iron availability in soil: interaction of Fe minerals, plants, and microbes, *J. Soils Sediments*, 2014, **14**, 538–548.

13 J. K. Fredrickson, J. M. Zachara, D. W. Kennedy, R. K. Kukkadapu, J. P. McKinley, S. M. Heald, C. Liu and A. E. Plymale, Reduction of TcO_4^- by sediment-associated biogenic Fe(II), *Geochim. Cosmochim. Acta*, 2004, **68**, 3171–3187.

14 J. Klausen, S. P. Troeber, S. B. Haderlein and R. P. Schwarzenbach, Reduction of substituted nitrobenzenes by Fe(II) in aqueous mineral suspensions, *Environ. Sci. Technol.*, 1995, **29**, 2396–2404.

15 C. A. Gorski and M. S. Fantle, Stable mineral recrystallization in low temperature aqueous systems: A critical review, *Geochim. Cosmochim. Acta*, 2017, **198**, 439–465.

16 R. Marsac, M. Pasturel and K. Hanna, Reduction kinetics of nitroaromatic compounds by titanium-substituted magnetite, *J. Phys. Chem. C*, 2017, **121**, 11399–11406.

17 D. E. Latta, C. A. Gorski, M. I. Boyanov, E. J. O'Loughlin, K. M. Kemner and M. M. Scherer, Influence of magnetite stoichiometry on U^{VI} reduction, *Environ. Sci. Technol.*, 2012, **46**, 778–786.

18 P. Dhakal, C. J. Matocha, F. E. Huggins and M. M. Vandiviere, Nitrite reactivity with magnetite, *Environ. Sci. Technol.*, 2013, **47**, 6206–6213.

19 C. A. Gorski, R. M. Handler, B. L. Beard, T. Pasakarnis, C. M. Johnson and M. M. Scherer, Fe atom exchange between aqueous Fe^{2+} and magnetite, *Environ. Sci. Technol.*, 2012, **46**, 12399–12407.

20 A. J. Frierdich, B. L. Beard, M. M. Scherer and C. M. Johnson, Determination of the Fe(II)aq–magnetite equilibrium iron isotope fractionation factor using the three-isotope method and a multi-direction approach to equilibrium, *Earth Planet. Sci. Lett.*, 2014, **391**, 77–86.

21 R. M. Handler, B. L. Beard, C. M. Johnson and M. M. Scherer, Atom exchange between aqueous Fe(II) and goethite: An Fe isotope tracer study, *Environ. Sci. Technol.*, 2009, **43**, 1102–1107.

22 P. Larese-Casanova and M. M. Scherer, Fe(II) sorption on hematite: New insights based on spectroscopic measurements, *Environ. Sci. Technol.*, 2007, **41**, 471–477.

23 A. J. Frierdich, M. Helgeson, C. Liu, C. Wang, K. M. Rosso and M. M. Scherer, Iron Atom Exchange between Hematite and Aqueous Fe(II), *Environ. Sci. Technol.*, 2015, **49**, 8479–8486.

24 P. Joshi and C. A. Gorski, Anisotropic Morphological Changes in Goethite during Fe^{2+}-Catalyzed Recrystallization, *Environ. Sci. Technol.*, 2016, **50**, 7315–7324.

25 E. Silvester, L. Charlet, C. Tournassat, A. Géhin, J.-M. Grenèche and E. Liger, Redox potential measurements and Mössbauer spectrometry of Fe^{II} adsorbed onto Fe^{III} (oxyhydr) oxides, *Geochim. Cosmochim. Acta*, 2005, **69**, 4801–4815.

26 C. I. Pearce, O. Qafoku, J. Liu, E. Arenholz, S. M. Heald, R. K. Kukkadapu, C. A. Gorski, C. M. B. Henderson and K. M. Rosso, Synthesis and properties of titanomagnetite ($Fe_{3-x}Ti_xO_4$) nanoparticles: A tunable solid-state Fe(II/III) redox system, *J. Colloid Interface Sci.*, 2012, **387**, 24–38.

27 C. A. Gorski and M. M. Scherer, Fe^{2+} sorption at the Fe oxide-water interface: A revised conceptual framework, *Aquat. Redox Chem.*, 2011, **1071**, 315–343.

28 C. I. Pearce, C. M. B. Henderson, N. D. Telling, R. A. D. Pattrick, J. M. Charnock, V. S. Coker, E. Arenholz, F. Tuna and G. van der Laan, Fe site occupancy in magnetite-ulvöspinel solid solutions: A new approach using X-ray magnetic circular dichroism, *Am. Mineral.*, 2010, **95**, 425–439.

29 S. Gota, M. Gautier-Soyer and M. Sacchi, Fe 2p absorption in magnetic oxides: Quantifying angular-dependent saturation effects, *Phys. Rev. B: Condens. Matter Mater. Phys.*, 2000, **62**, 4187–4190.

30 R. A. D. Pattrick, G. Van Der Laan, C. M. B. Henderson, P. Kuiper, E. Dudzik and D. J. Vaughan, Cation site occupancy in spinel ferrites studied by X-ray magnetic circular dichroism, *Eur. J. Mineral.*, 2002, **14**, 1095–1102.

31 A. F. White and M. L. Peterson, Reduction of aqueous transition metal species on the surfaces of Fe(II)-containing oxides, *Geochim. Cosmochim. Acta*, 1996, **60**, 3799–3814.

32 C. A. Gorski, R. Edwards, M. Sander, T. B. Hofstetter and S. M. Stewart, Thermodynamic characterization of iron oxide–aqueous Fe^{2+} redox couples, *Environ. Sci. Technol.*, 2016, **50**, 8538–8547.

33 E. Tronc, J. P. Jolivet, P. Belleville and J. Livage, Redox phenomena in spinel iron oxide colloids induced by adsorption, *Hyperfine Interact.*, 1989, **46**, 635–643.

34 B. R. Coughlin and A. T. Stone, Nonreversible adsorption of divalent metal ions (Mn^{II}, Co^{II}, Ni^{II}, Cu^{II}, and Pb^{II}) onto goethite: Effects of acidification, Fe^{II} addition, and picolinic acid addition, *Environ. Sci. Technol.*, 1995, **29**, 2445–2455.

35 P. J. Vikesland, R. L. Rebodos, J. Y. Bottero, J. Rose and A. Masion, Aggregation and sedimentation of magnetite nanoparticle clusters, *Environ. Sci.: Nano*, 2016, **3**, 567–577.

36 Y. You, S. Zheng, H. Zang, F. Liu, F. Liu and J. Liu, Stimulatory effect of magnetite on the syntrophic metabolism of Geobacter co-cultures: Influences of surface coating, *Geochim. Cosmochim. Acta*, **2018**, DOI: 10.1016/j.gca.2018.1002.1009.

37 C. A. Gorski and M. M. Scherer, Determination of nanoparticulate magnetite stoichiometry by Mössbauer spectroscopy, acidic dissolution, and powder X-ray diffraction: A critical review, *Am. Mineral.*, 2010, **95**, 1017–1026.

38 Y. Mamindy-Pajany, C. Hurel, N. Marmier and M. Roméo, Arsenic (V) adsorption from aqueous solution onto goethite, hematite, magnetite and zero-valent iron: Effects of pH, concentration and reversibility, *Desalination*, 2011, **281**, 93–99.

39 J.-P. Jolivet and E. Tronc, Interfacial electron transfer in colloidal spinel iron oxide. Conversion of Fe_3O_4-γFe_2O_3 in aqueous medium, *J. Colloid Interface Sci.*, 1988, **125**, 688–701.

40 S. V. Yanina and K. M. Rosso, Linked Reactivity at Mineral-Water Interfaces Through Bulk Crystal Conduction, *Science*, 2008, **320**, 218–222.

41 J. G. Catalano, P. Fenter, C. Park, Z. Zhang and K. M. Rosso, Structure and oxidation state of hematite surfaces reacted with aqueous Fe(II) at acidic and neutral pH, *Geochim. Cosmochim. Acta*, 2010, **74**, 1498–1512.

42 S. C. Pang, S. F. Chin and M. A. Anderson, Redox equilibria of iron oxides in aqueous-based magnetite dispersions: Effect of pH and redox potential, *J. Colloid Interface Sci.*, 2007, **311**, 94–101.

43 J. M. Byrne, N. Klueglein, C. Pearce, K. M. Rosso, E. Appel and A. Kappler, Redox cycling of Fe(II) and Fe(III) in magnetite by Fe-metabolizing bacteria, *Science*, 2015, **347**, 1473–1476.